10705
NACA TN 4361

TECH LIBRARY KAFB, NM
0067173

NATIONAL ADVISORY COMMITTEE FOR AERONAUTICS

TECHNICAL NOTE 4361

IDEALIZED WINGS AND WING-BODIES AT A MACH NUMBER OF 3

By Elliott D. Katzen

Ames Aeronautical Laboratory
Moffett Field, Calif.

Washington
July 1958

AFMDC
TECHNICAL LIBRARY

TECH LIBRARY KAFB, NM
0067173

NATIONAL ADVISORY COMMITTEE FOR AERONAUTICS

TECHNICAL NOTE 4361

IDEALIZED WINGS AND WING-BODIES AT A MACH NUMBER OF 3

By Elliott D. Katzen

The purpose of this paper is to describe the theoretical possibilities for obtaining high lift-drag ratios at $M = 3$ and to describe some experiments which were designed to exploit the theory. In discussing the theoretical maximum lift-drag ratios of idealized arrangements, it is convenient to consider, as a standard of comparison, the lifting flat plate. In figure 1 are shown the maximum lift-drag ratios for flat plates having two types of plan forms, the delta and the arrow. (For definitions of symbols, see appendix.) The maximum lift-drag ratios have been computed for $M = 3$ and for an assumed minimum drag coefficient of 0.005. This value of minimum drag coefficient corresponds to that for a very large airplane flying at a high Reynolds number so that the friction drag coefficient would be relatively low. The maximum lift-drag ratios are shown as a function of the slenderness parameter $\beta \tan \epsilon$ where β is defined as $\sqrt{M^2-1}$ and ϵ is the semiapex angle of the leading edge of the wing. In addition to the results for flat plates, the improvement in lift-drag ratio predicted by cambering and twisting the wings is shown. For both types of plan forms with supersonic leading edges and for the subsonic leading-edge delta wings, the drag-due-to-lift results of references 1 and 2 were used to compute the improved lift-drag ratios. For the arrow wings with subsonic leading edges, the drag due to lift was optimized by using a four-term load distribution in the manner of references 3 and 4. The calculations were made at one point, $\beta \tan \epsilon = 0.5$. The curve of lift-drag ratio was then faired from this calculated point to the points calculated for arrow wings with supersonic leading edges.

It can be seen from figure 1 that $(L/D)_{max}$ for the arrow wings is higher than that for the delta wings. The improvement caused by warping decreases as the slenderness is decreased, and for wings with highly supersonic leading edges the improvement becomes negligible. These trends would be the same if a higher minimum drag coefficient had been assumed, but the magnitudes would be different. For example, if $C_{D_o} = 0.015$ had been chosen, the $(L/D)_{max}$ for the very slender arrow wing would be about 7 instead of over 11, as shown in figure 1. For the very slender arrow wing, $\beta \tan \epsilon = 0.5$, relatively high lift-drag ratios are predicted. Experiments were designed then in an attempt to attain this high lift-drag ratio.

Four models are shown in figure 2 which were cambered and twisted for low drag due to lift. (See refs. 3 and 4.) Models 1 and 2 were designed for a lift coefficient of 0.1; the wings are rather extreme, as can be seen from sections taken at various stations along the wing. The forward part of the wing is raised considerably above the $Z = 0$ plane.

Since the trailing edge of the root chord lies in the $Z = 0$ plane, the resulting angle of attack of the root section is relatively high, about 7.5°, compared with the tips which are at about zero angle of attack. Model 2 has the same camber and twist as model 1, but the dihedral has been changed in an attempt to change the separation pattern on the wing. At the 7-inch station it is seen that model 2 is turned below the $Z = 0$ plane, compared with model 1 which is above the $Z = 0$ plane. This change in dihedral with no changes of camber and twist leaves the forward part of the wing "dished out." One method of adding volume to the wing is, therefore, suggested, and model 3 is simply model 2 with volume added to fill the dished-out region. Model 4 was designed for a lift coefficient of 0.05. The optimum lift is, therefore, to be obtained half by camber and twist and half by angle of attack. The wing is less extreme than that of the previous models; the forward portion is only half as far above the $Z = 0$ plane as is model 3. The wings, except for model 3, have 12-percent-thick sections normal to the leading edge. The wing section used, normal to the leading edge, is the Clark Y. For the models shown, the symmetrical part of the Clark Y (above and below the Clark Y mean line) was wrapped around the calculated mean lines. The resulting sections, in the stream direction, are about 3.4 percent thick. With this thickness, for this very slender shape, the wings resemble bodies more than wings, especially in the forward region.

Experimental results for models 1 and 4 are shown in figures 3 and 4. It can be seen in figure 3 that reducing the design lift coefficient reduces the lift at a fixed angle of attack with little change in lift-curve slope. The less extreme wing (model 4) has less drag than the wing designed for a lift coefficient of 0.1 (model 1). It can be seen that with the pitching moments taken about an axis at 35 percent of the mean aerodynamic chord, model 1 trims at the optimum lift coefficient. Model 4, however, trims at a lower lift coefficient; therefore, a control surface or flap would have to be deflected, and a trim drag penalty would result. Both models are stable throughout the test range of lift coefficients, but there is a tendency toward neutral stability at the higher lift coefficients.

Figure 4 shows that the maximum lift-drag ratio for model 4, the less extreme wing, is 8.4 compared with about 7.4 for model 1 which was designed for a lift coefficient of 0.1. Model 2, also designed for a lift coefficient of 0.1, had a different separation pattern but had about the same maximum lift-drag ratio as model 1. Increasing the volume of model 2, as shown in figure 2, reduced the maximum lift-drag ratio from 7.4 to about 6.0. Calculated drag coefficients for models 1 and 4 at their design lift coefficients are shown by solid symbols (fig. 3). Calculated maximum lift-drag ratios are shown in the same manner (fig. 4). It is seen that for the wing designed for a lift coefficient of 0.05, theory and experiment are in good agreement at the design point. This is not the case for the wing designed for a lift coefficient of 0.1.

The results shown in figures 3 and 4 are for the maximum test Reynolds number of 3.5×10^6, based on the wing mean aerodynamic chord. At this Reynolds number and lower test Reynolds numbers separation occurs on the wing as shown in figure 5. In this figure, results of visual-flow studies made by using the liquid-film and vapor-screen techniques are presented. The pattern of a film of white lead applied to the upper surfaces of model 1 shows two rows of bubbles, indicating separation, near the leading edge and further inboard. Sketches made from vapor-screen studies also indicate separation. In the vapor-screen technique, light is made to shine through the wind-tunnel windows in a plane perpendicular to the model axis. Water vapor introduced into the wind tunnel shows regions of separation and vortices as dark areas in the plane of light. Regions of separation for the light plane near the midchord station of the model are shown in figure 5. The separated region approximately corresponds to the area between the two rows of bubbles seen in the liquid-film pattern. Further downstream the region of separation is wider and raised higher off the wing. Still further downstream, the separated flow rolls up into discrete vortices.

Calculations made by C. E. Brown of the Langley Laboratory indicate that even for the very slender wing with a Mach number normal to the leading edge of 0.5, the local Mach number on the upper surface of the wing exceeds the critical Mach number. Thus, transonic effects including shock waves may combine with viscous effects and cause the separation shown on the wing. Supersonic wing theory, the basis for the design of the wings studied, does not take account of these effects, and differences between theory and experiment are thus to be expected.

Additional visual-flow studies using sublimation and shadowgraph techniques indicate that the boundary layer was turbulent on both upper and lower surfaces of the wing except for a narrow region (enough to support laminar separation) near the leading edge. For these highly sweptback wings the transition pattern was constant for the angle-of-attack and Reynolds number ranges of the tests; thus, the results presented herein are for an essentially turbulent boundary layer.

Figure 6 shows two wings, models 5 and 6, of the same plan form as the previous models, but the camber and twist are different. Model 5 is untwisted and has a cambered wing section. The section normal to the leading edge is the Clark Y (12 percent thick). Model 6 is the same wing twisted in the direction indicated by theory for the previous models; the tips are "washed out."

The experimental results for models 5 and 6 are presented in figures 7 and 8. It can be seen in figure 7 that washing out the tips reduces the lift at fixed angles of attack with little change in lift-curve slope. There is also little change in the minimum drag coefficient, but the drag polar is shifted and, therefore, the maximum lift-drag ratio is increased from 8.4 to 9 (fig. 8). Twisting the wing had a large effect

on the pitching moments; for the untwisted wing there would be a drag penalty involved in trimming the wing. The twisted wing trims at optimum lift coefficient.

The effect of adding volume to model 6 is shown in figure 9. Model 6 (the wing alone) has a large volume. If the wing had as large an area as is currently being considered for some airplanes, for example, 5,000 or 6,000 square feet, the volume would be about 10,000 cubic feet, almost that of the Boeing B-52 fuselage. Volume was added to model 6 by placing the wing on a circular-cylindrical body and also by placing wedges under the wing in order to obtain favorable interference lift at the same time the volume was increased. The wedge height for the model shown is 4 percent of the total wing length. In addition, the wing was tested with a wedge having a height of 2 percent of the total wing chord. The maximum lift-drag ratio and volume for the latter wing-wedge model were approximately the same as for the wing with the circular-cylindrical body.

In figure 10 the calculated and experimental maximum lift-drag ratios for model 6 are shown as a function of Reynolds number. The only change with Reynolds number in the calculated curve is the result of skin friction. Unpublished experimental results, which are in close agreement with the T' method of Rubesin and Johnson as presented in reference 5, for turbulent boundary layers were used in the calculations. Also shown in figure 10 is a calculation in which a drag increment is added to that of model 6, and then the results are extrapolated to high Reynolds numbers in a manner to be expected from skin-friction considerations. The added drag increment includes an estimated allowance for vertical fins to provide directional stability and for nacelles. It can be seen from figure 10 that the experimental lift-drag ratios for model 6 increase at a faster rate with increasing Reynolds number than is to be expected from skin-friction considerations alone. It is believed that this increased rate is caused by changes in separation effects as the Reynolds number is increased.

In summary, it is seen that the relatively high lift-drag ratios calculated were partly realized at low wind-tunnel Reynolds numbers. An experimental trimmed lift-drag ratio of 9 was obtained instead of the estimated value of 11. The rate of increase in maximum lift-drag ratio with increased Reynolds number, however, was greater than expected, thereby indicating the desirability of further experiments at conditions closer to actual flight.

Ames Aeronautical Laboratory
National Advisory Committee for Aeronautics
Moffett Field, Calif., Mar. 20, 1958

APPENDIX

SYMBOLS

c	wing root chord
$\bar{c}$	wing mean aerodynamic chord
C_D	drag coefficient
C_{D_o}	drag coefficient caused by air friction and wave production due to volume
C_L	lift coefficient
C_m	pitching-moment coefficient
$\frac{L}{D}$	ratio of lift to drag
M	Mach number
R	Reynolds number based on wing mean aerodynamic chord
Z	wing ordinate measured from horizontal plane passing through trailing edge of wing root chord
α	angle of attack
β	$\sqrt{M^2-1}$
ϵ	semiapex angle of the wing leading edge

Subscripts

des	design conditions
max	maximum

REFERENCES

1. Zhilin, Yu. L.: Wings of Minimum Drag. Prikladnaia Matematika i Mekhanika (Moscow, Leningrad), vol. XXI, 1957, pp. 213-220.

2. Cohen, Doris: The Warping of Triangular Wings for Minimum Drag at Supersonic Speeds. Jour. Aero. Sci. (Readers' Forum), vol. 24, no. 1, Jan. 1957, pp. 67-68.

3. Tucker, Warren A.: A Method for the Design of Sweptback Wings Warped to Produce Specified Flight Characteristics at Supersonic Speeds. NACA Rep. 1226, 1955. (Supersedes NACA RM L51F08)

4. Grant, Frederick C.: The Proper Combination of Lift Loadings for Least Drag on a Supersonic Wing. NACA Rep. 1275, 1956. (Supersedes NACA TN 3533)

5. Sommer, Simon C., and Short, Barbara J.: Free-Flight Measurements of Turbulent-Boundary-Layer Skin Friction in the Presence of Severe Aerodynamic Heating at Mach Numbers From 2.8 to 7.0. NACA TN 3391, 1955.

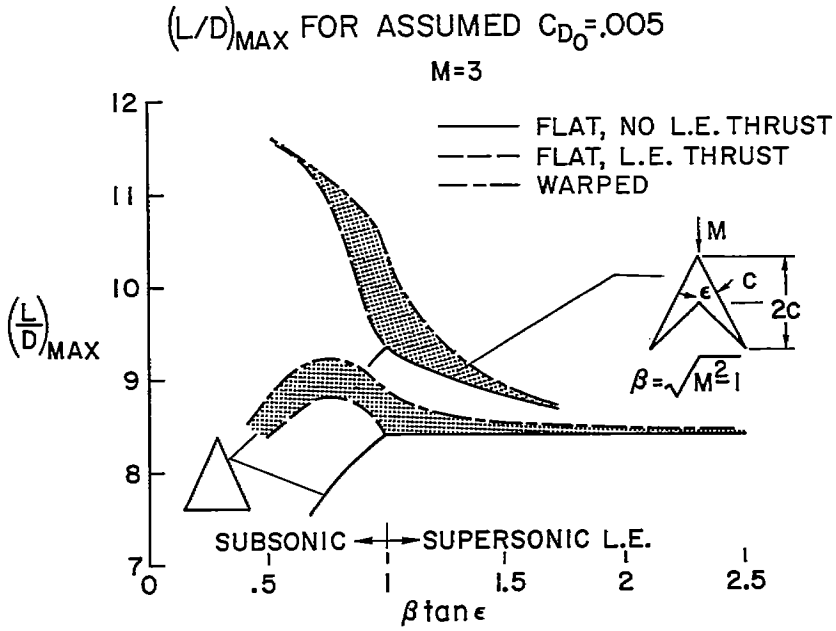

Figure 1

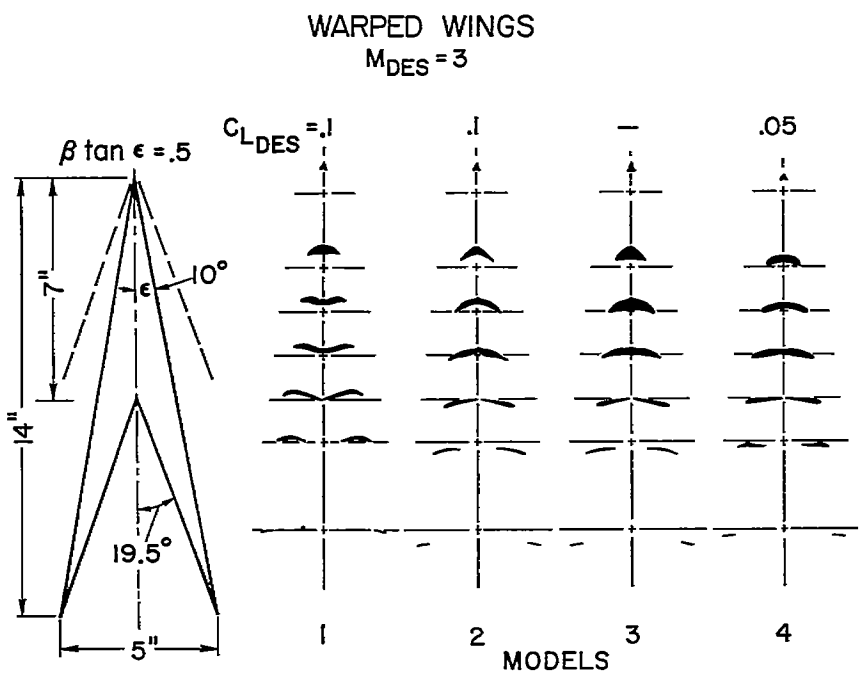

Figure 2

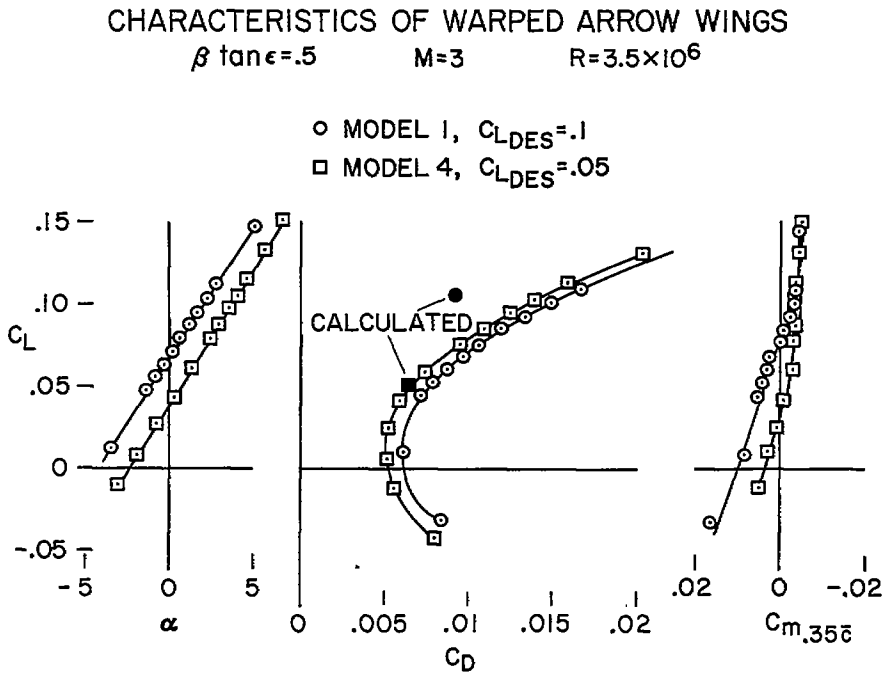

Figure 3

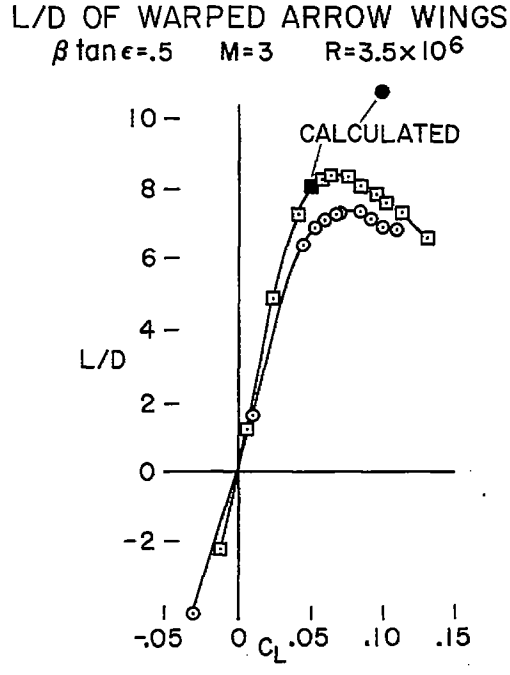

Figure 4

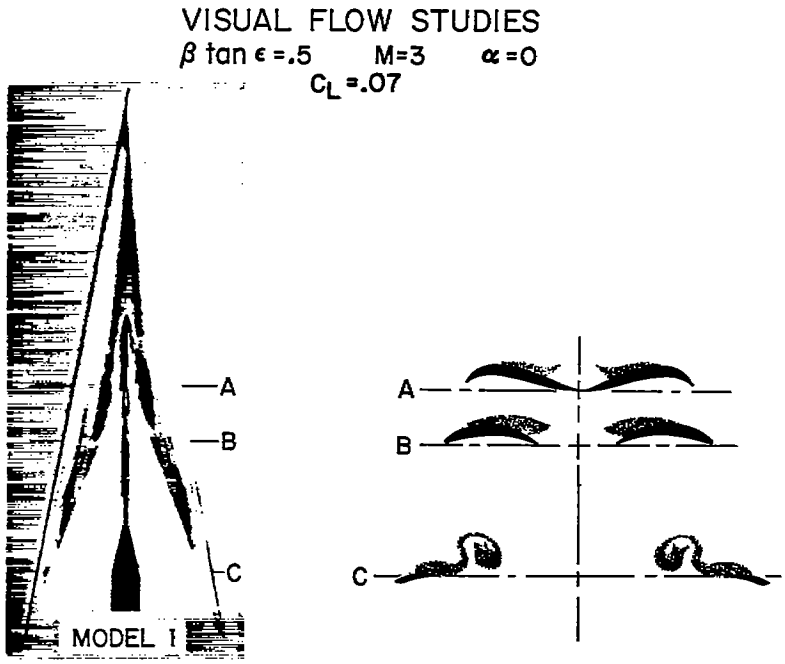

Figure 5

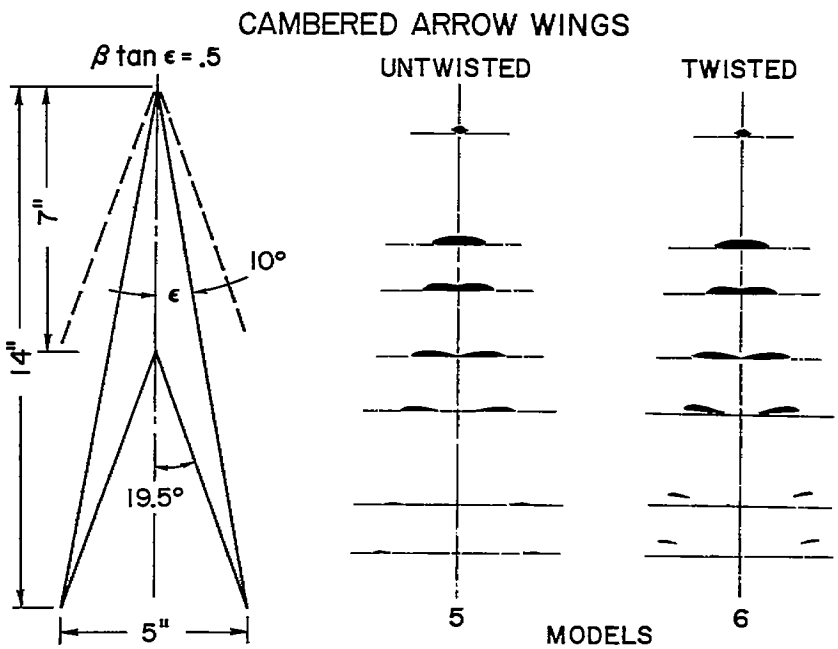

Figure 6

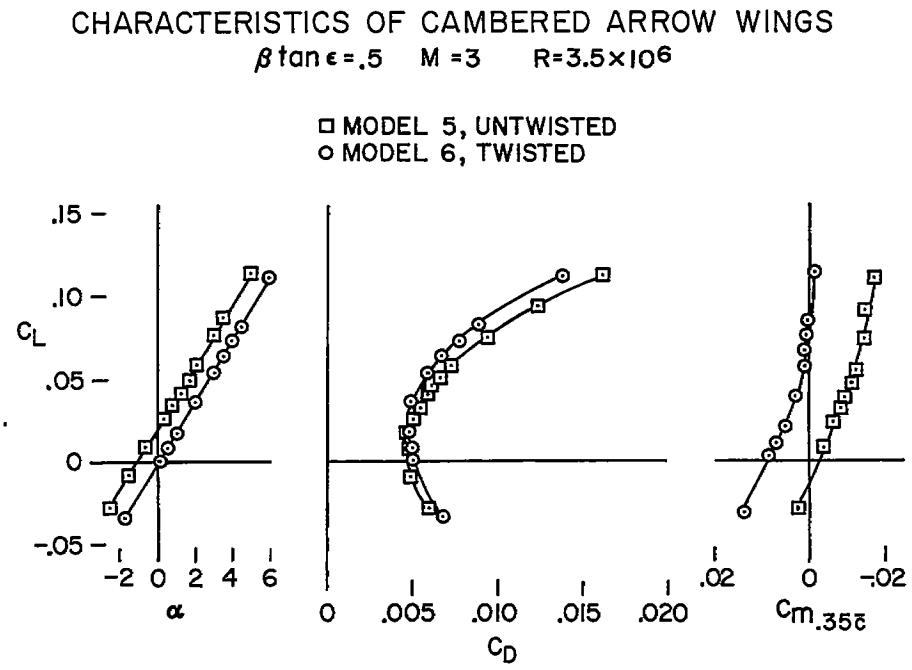

Figure 7

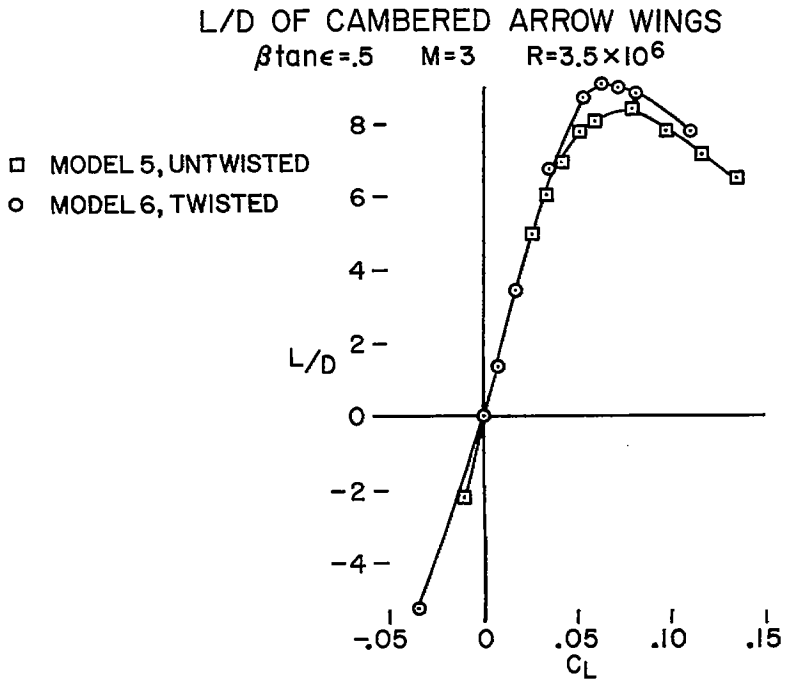

Figure 8

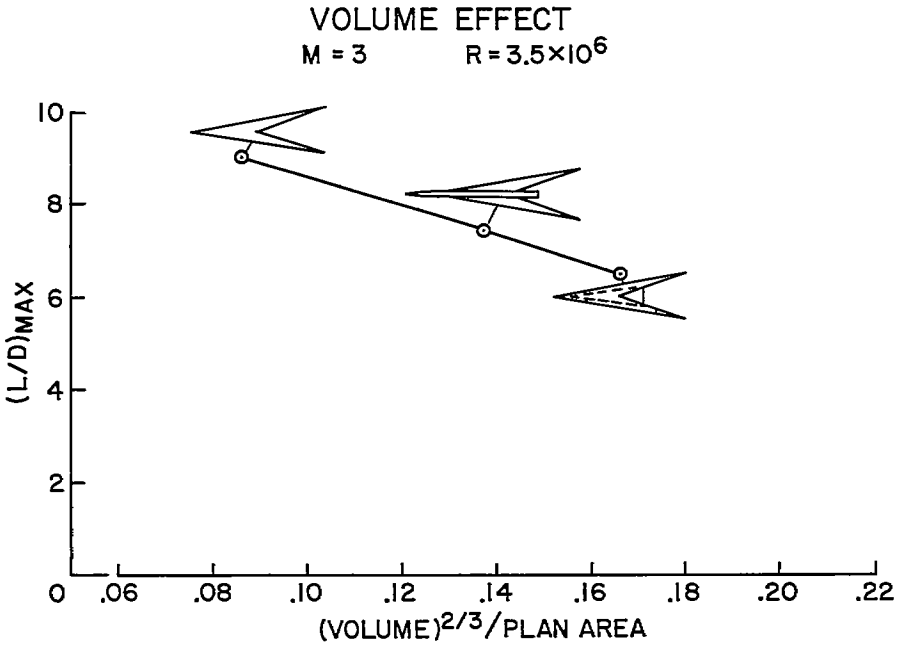

Figure 9

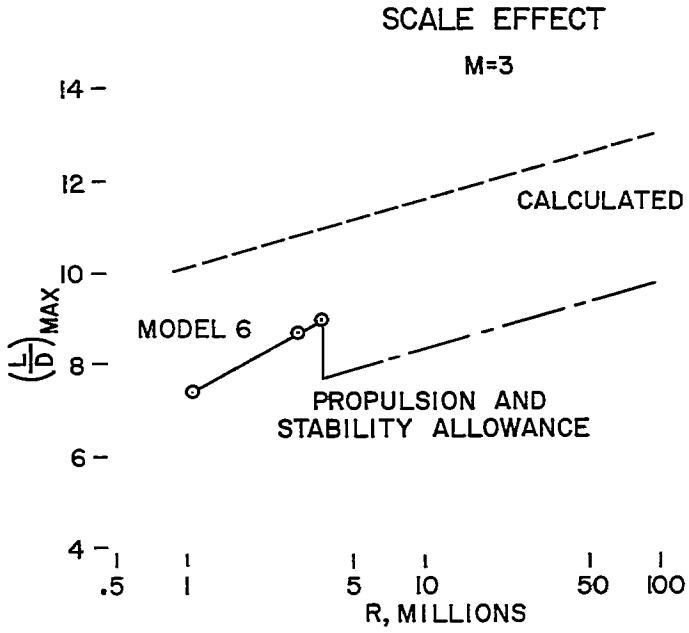

Figure 10